RAPID COMMUNICATION

Electrically controlled atomic writing and emergent properties in $YCoO_3$ films

Kui Chu(褚奎)[1,2,†], Huayu Tao(陶花语)[2,3,†], Xiangyu Lyu(吕翔宇)[2,3], Jin Liu(刘锦)[2,4,‡], Ailing Ji(纪爱玲)[2,4], Guopeng Wang(王国鹏)[1,§], and Nianpeng Lu(鲁年鹏)[2,4,¶]

[1] *School of Physics, Anhui University, Hefei* 230601, *China*
[2] *Beijing National Laboratory for Condensed Matter Physics, Institute of Physics, Chinese Academy of Sciences, Beijing* 100190, *China*
[3] *College of Materials Science and Opto-Electronic Technology, University of Chinese Academy of Sciences, Beijing* 101408, *China*
[4] *School of Physical Sciences, University of Chinese Academy of Sciences, Beijing* 100190, *China*

(Received 28 May 2026; revised manuscript received 22 June 2026; accepted manuscript online 29 June 2026)

On the demands of high-precision and reconfigurable fabrication of nano-electronic devices, this work adopts the scanning probe-based modulation technique to achieve mask-free high-resolution nanopatterning and reversible hydrogen writing on $YCoO_3$ thin films. By precisely controlling the electric bias, the intense electric field produced by the atomic probe can electrically catalyze and drive the directional migration and selective intercalation of hydrogen ions, thereby enabling localized modulation of the lattice and electrical properties of $YCoO_3$ thin films with the best spatial resolution of 100 nm. Direct hydrogen writing by the atomic probe induces an obvious out-of-plane lattice expansion, decreased electrical conductivity, and obvious optical contrast. Moreover, the modified $YCoO_3$ thin films possess excellent thermal stability and demonstrate very nice erasing–writing reversibility. By leveraging the strong ion–lattice–charge coupling in $YCoO_3$ systems, this work provides a powerful reconfigurable strategy for the fabrication and integration of high spatial resolution and high-throughput electronic devices.

Keywords: $YCoO_3$ films, atomic probe writing, hydrogen modulation, electrical properties

PACS: 68.47.Gh, 71.30.+h, 68.37.Ps, 88.20.fn, 81.16.Rf

DOI: 10.1088/1674-1056/ae838f **CSTR:** 32038.14.CPB.ae838f

1. Introduction

In correlated electron systems,[1–5] the strong coupling among different degrees of freedom can significantly modify the band energy distribution and electronic state evolution dynamics, giving rise to many exotic physical properties, such as metal–insulator transition, intriguing magnetic ordering and even superconductivity, which represent the core scientific focuses in condensed matter physics and material sciences.[6–11] Owing to their unique electronic structures and tunable physical properties, oxide materials exhibit promising prospects in low-temperature electronics, quantum information, sensor detection and energy conversion, serving as an essential material platform for developing high-performance and reconfigurable electronic devices.[8,12,13]

As a typical rare-earth cobalt-based perovskite oxide, $YCoO_3$ (YCO) shares a similar crystal structure and electronic configuration with other oxide materials, such as $LaCoO_3$.[14–19] Benefiting from the small ionic radius of the A-site Y ion and the large oxygen octahedra distortion, YCO possesses lower ionic migration barriers, enabling significant ion diffusion and migration at low temperatures. Compared with other cobalt-based oxides, it exhibits unique ionic transport characteristics and structural tunability.[4,20–25] Therefore, it is an ideal candidate material for the research of ionic modulation. Recent studies have verified that hydrogen atmosphere annealing can achieve hydrogenation of YCO thin films to form stable new phases of $HYCoO_3$ (HYCO),[26] accompanied by obvious lattice expansion, band gap variation, and electrical property modulation. However, conventional hydrogen annealing only enables global modification of materials and fails to realize localized, precise, and reversible hydrogen distribution at the nanoscale that is required in the fabrication of high-density, high-resolution, and reconfigurable nanodevices.[13,27–32]

In recent years, atomic-probe-based electric field modulation has proved to be an effective approach to address the above challenges.[29,33–35] It enables precise regulation of lattice structure, electronic and magnetic properties at the atomic scale, providing an effective strategy for designing high-performance functional devices. By applying a controllable bias between the probe and the sample surface, a

[†]These authors contribute equally to this work.
[‡]Corresponding author. E-mail: liujin@iphy.ac.cn
[§]Corresponding author. E-mail: gpwang@ahu.edu.cn
[¶]Corresponding author. E-mail: lunianpeng@iphy.ac.cn

© 2026 Chinese Physical Society and IOP Publishing Ltd. All rights, including for text and data mining, AI training, and similar technologies, are reserved.

CPB Online In Press

highly localized intense electric field could induce electrolysis of surface-adsorbed water molecules in ambient conditions or catalytic decomposition of hydrogen gas in a controlled environment, and drive the produced hydrogen ions or protons to intercalate into the structural lattice of materials.[16,36–40] This enables in-situ, mask-free and low-damage localized modulation of lattice structures, electronic states and even macroscopic physical properties. Such modulation has been verified in various material systems, showing prominent advantages such as high spatial resolution, repeatable erasable-writable performance and environmental friendliness.[41,42]

In this work, the YCO film is employed as the model material system for local hydrogen modulation and mask-free nanopatterning. Through electrically controlled atomic probe writing, reversible structural and electrical regulation was achieved, and the associated ion–lattice–charge couplings were also clarified. Local hydrogen modulation can effectively induce lattice expansion and significantly affect the electrical behaviors of the film, while exhibiting excellent thermal stability, spatial resolution, and cycling reversibility. This work provides a reliable basis for fabricating nanoelectronic devices, such as high-density neuromorphic arrays and reconfigurable electronic circuits.

2. Experimental details

YCO (110) films were grown on $YAlO_3$ (110) substrates via the pulsed laser deposition method. The growth parameters were set as a substrate temperature of 600 °C, an oxygen partial pressure of 25 Pa, and a repetition frequency of 2 Hz. After deposition, the samples were annealed in a pure oxygen atmosphere for 30 min, and then cooled down to room temperature at a cooling rate of 15 °C/min. Finally, YCO films with a thickness of approximately 40 nm were obtained. The crystallinity and surface morphology of the films were characterized by x-ray diffraction (XRD) and atomic force microscopy (AFM).

Atomic probe writing was carried out on a scanning probe microscope (SPM, MFP Origin 3D) equipped with a conductive module and an atmosphere-controlled chamber. Platinum-coated conductive probes with a curvature radius of $\sim$ 10 nm were used, and the modulation was implemented in a mixed atmosphere of 5% H_2 and 95% Ar. Through platinum probe H_2 catalysis and under a positive bias ranging from 0 to +7 V, the localized hydrogenation of the YCO film can be realized. In contrast, hydrogen can be extracted under a negative bias of −7 V to achieve reversible dehydrogenation. Nanoscale writing was implemented by programmatically controlling scanning paths, bias amplitudes, and scanning speeds (520 μm/s). A conductive atomic force microscope (c-AFM) was employed to measure the local conductivity and current–voltage (I–V) characteristics.

3. Results and discussion

3.1. Hydrogen induced phase transition and electric-controlled probe writing

To verify the feasibility of Pt-assisted catalytic hydrogenation in YCO thin films, isolated Pt nanoparticles were deposited on the sample surface. Subsequently, the samples were annealed at 100 °C for 10 min in flowing forming gas consisting of 5% H_2 and 95% Ar, as shown in Fig. 1(a). An obvious phase transition from pristine YCO to hydrogenated HYCO can be observed. The lattice expansion derived from the XRD peak shift after hydrogen doping is approximately 4.7%.

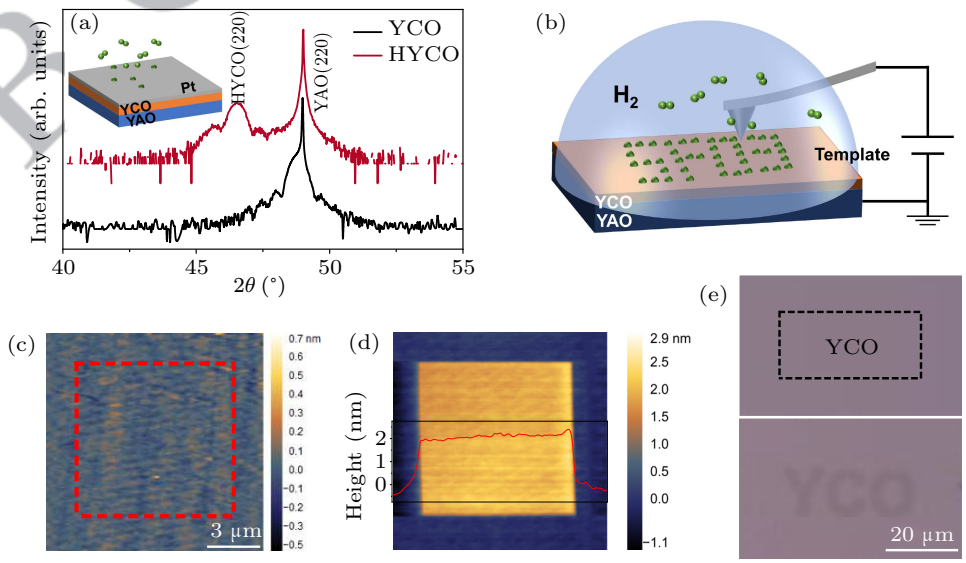


Fig. 1. Hydrogen doping effects for the YCO thin films. (a) XRD patterns of the thin films before and after hydrogenation, and the inset shows the spillover hydrogenation method. (b) Schematic diagram of electrically controlled probe writing on YCO thin films. (c) Surface morphology of the thin film characterized by AFM before probe writing. (d) Lattice expansion behavior of the thin films after tip-induced hydrogen doping. (e) Tip-written pattern on the YCO thin film. Distinct optical contrast between the pristine (upper) and written (lower) regions verifies the successful hydrogenation, in which a voltage (top panel, 10 V) is adopted for tip patterning.

CPP Online In-Press

To confirm the AFM tip induced hydrogen ion migration in YCO thin films, Pt-coated conductive probes were used, as schematically shown in Fig. 1(b). Inside the SPM chamber, the Pt probe efficiently promotes the dissociation of hydrogen molecules into protons. Meanwhile, a positive bias voltage applied between the probe and sample drives protons to intercalate into the YCO film and form hydrogenated HYCO phase. In this process, the electrons are synchronously supplied through external circuits to maintain charge neutrality of the system. Benefiting from the precise control capability of the SPM technique, the hydrogenation reaction is confined to the region between probe and sample, enabling nanoscale spatial modulation of YCO thin films.

To quantify the effective modulation, an area of 10×10 μm^2 on the film surface was selected for AFM writing. Clear terraced structures are observed (Fig. 1(c)), confirming the high quality of deposited films. Direct atomic probe writing was performed at the central region of the selected area, and an obvious height variation was detected. By comparing the height variation with the film thickness, the lattice expansion after hydrogen intercalation was determined to be about 5%, which is consistent with the lattice expansion value calculated from XRD results (Fig. 1(d)). Figure 1(e) presents the optical contrast change on the YCO film (bottom panel) after writing the preset pattern (top panel). The result demonstrates the clear optical transmittance contrast of the HYCO phase embedded in the pristine YCO film. The scanning voltage was set to 10 V for the large scanned area to achieve effective hydrogen doping, which enables a clearer visualization of the phase-transitioned regions under the optical microscope.

3.2. Atomic writing modulated surface morphology and electric conductivity

To further elucidate the intrinsic coupling among proton intercalation, lattice deformation, and electronic transport behavior, the c-AFM measurements were conducted on both pristine YCO and locally hydrogenated HYCO regions to distinguish the conductivity variation of the films. During the writing process, different bias voltages were applied through the Pt-coated conductive tip, enabling controllable local proton injection and therefore continuously tunable hydrogen doping concentrations.

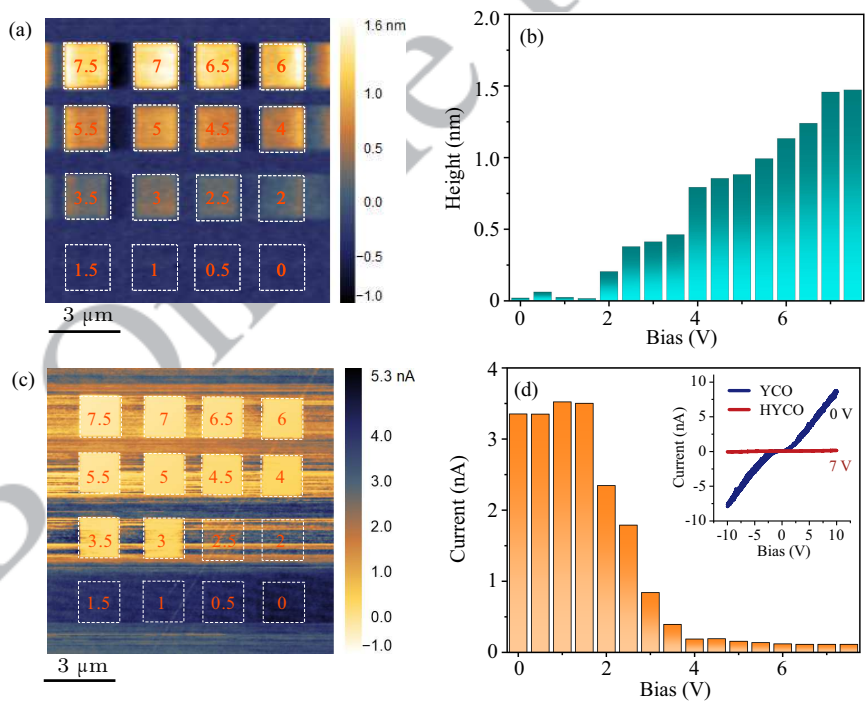


Fig. 2. Micropatterning via local hydrogen intercalation. (a) Microscopic profiles of pristine YCO and HYCO, where nanoscale lattice expansion is clearly observed. (b) Height variation of lattice expansion extracted from (a) with different writing voltages. (c) c-AFM current mapping showing conductivity modulation between pristine YCO and hydrogenated HYCO regions. (d) Electric conductance statistics extracted from (c). Pristine YCO shows high conductance, whereas HYCO exhibits suppressed conductivity. The inset displays the measured *I*–*V* curves of the pristine and modulated regions at the written voltage of 7 V.

Figure 2(a) presents the topographic images of nanoscale square patterns written under different tip biases, and the corresponding statistical height analysis is summarized in Fig. 2(b). A clear monotonic increase in surface protrusion height with increasing writing voltage is observed, indicating that higher electric fields promote more efficient proton incorporation into the lattice. Notably, the threshold voltage appears to be between 1.5 V and 2 V. Below this voltage, negligible topographic variation is detected. Once the applied bias exceeds the threshold voltage, the expansion height increases accordingly with voltage, revealing the activation of the protonation process. Furthermore, the lattice expansion gradually approaches saturation at approximately 7 V, where the height change tends to stabilize. This saturation behavior implies that

the available proton intercalation sites in the near-surface region become nearly fully occupied, or that the proton injection efficiency reaches its upper limit under the present experimental conditions. The nearly linear dependence of height expansion on applied bias within the intermediate writing voltage range suggests that the proton concentration can be quantitatively modulated by the local electric field.

The corresponding current mapping of the same pattern region is displayed in Fig. 2(c), with the extracted current summarized in Fig. 2(d). In contrast to the surface morphology change, the hydrogenated regions exhibit a pronounced suppression of local current, revealing a substantial increase in electrical resistance after proton intercalation. Furthermore, the current decreases systematically as the writing voltage increases, indicating that the strength of conductivity modulation is strongly correlated with the proton doping level. The reduction in conductance can be attributed to proton-induced modification of the Co valence state and accompanying lattice expansion, which weaken electron hopping with enhanced carrier localization.[16,17] From the above results, we know that even at the nanoscale the structural lattice distortion and electronic phase transition were strongly coupled in the hydrogenation process.

To quantitatively evaluate the electronic state evolution before and after hydrogenation, representative *I*–*V* curves measured on pristine YCO and hydrogenated HYCO regions are presented in the inset of Fig. 2(d). Compared to the conductive response of pristine YCO, the HYCO exhibits a strongly suppressed current over the entire bias range, confirming the significant increase in electric resistance. The continuously tunable electrical contrast observed here further demonstrates that the tip-assisted hydrogen intercalation approach can act as an effective pathway for deterministic nanoscale manipulation of oxide electronic states. These results collectively establish a direct correlation among local proton concentration, lattice deformation, and electrical transport modulation, providing important insights into proton-mediated ion–charge coupling in correlated oxides.

3.3. Stability test of the written patterns

To evaluate the practical applicability of locally protonated YCO for micro/nano-electronic and neuromorphic applications, the thermal stability, environmental robustness, and spatial confinement of written regions were systematically investigated. In particular, the retention behavior of proton-induced lattice expansion was examined under different

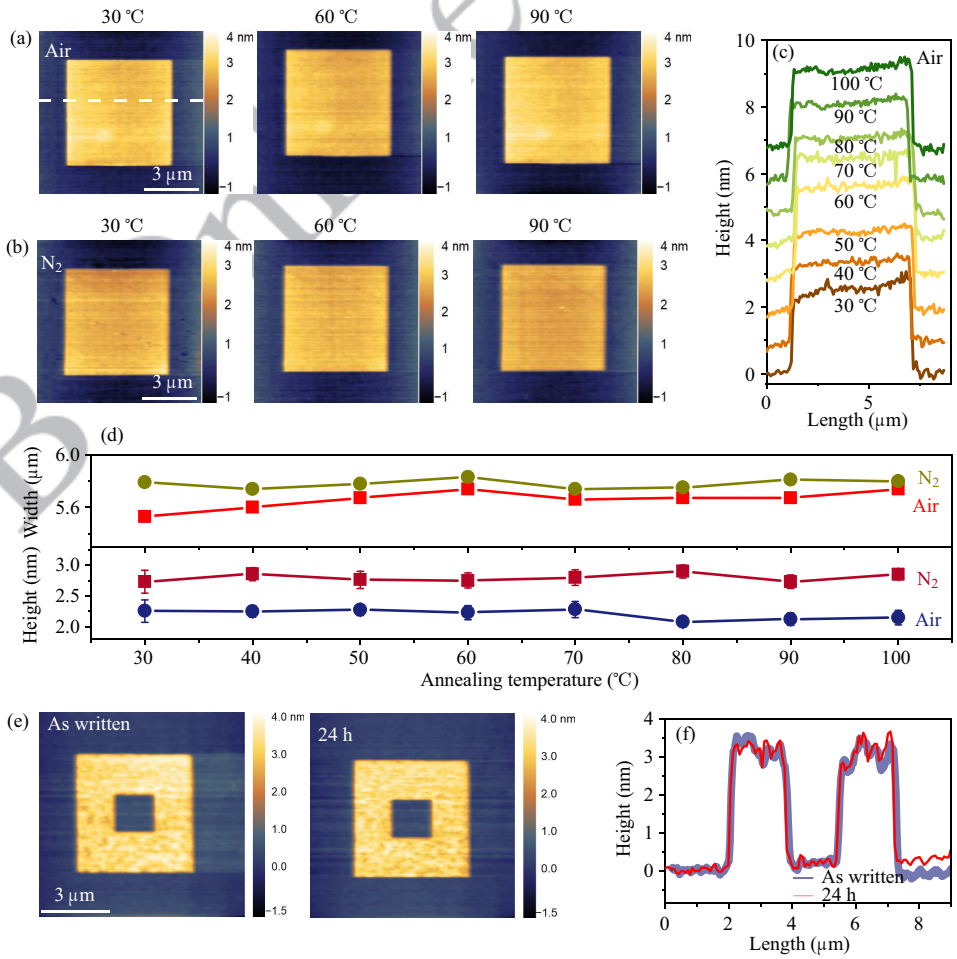


Fig. 3. Thermal and time dependent stability of the modulated samples. (a), (b) Morphological evolution of HYCO from 30 °C to 90 °C in air (a) and N_2 (b). (c) Summarized width variation of HYCO from 30 °C to 100 °C in air, with the data extracted from (a). (d) Height and width variation of HYCO from 30 °C to 100 °C in air and N_2. (e) Morphological comparison of HYCO before and after storage in air for 24 hours. (f) Height comparison of HYCO before and after exposure in air with the data extracted from (e). The curves are horizontally shifted together for comparison.

CPB Science Press

atmospheres and elevated temperatures to clarify the stability of intercalated YCO. A square pattern was first written on the YCO surface using an AFM tip, followed by stepwise thermal annealing from 30 °C to 100 °C in 10 °C increments, with a dwell time of 10 min at each temperature. As shown in Fig. 3(a), the written regions retain a clear topographic contrast throughout the heating process in air. No noticeable degradation of the pattern geometry or reduction in expansion height was observed even at 100 °C, indicating excellent thermal stability of the protonated state under ambient conditions. The result suggests that the incorporated protons are strongly confined within the lattice rather than weakly adsorbed on the surface.

To distinguish intrinsic lattice stabilization from possible environmental effects, identical thermal experiments were further performed under an N_2 atmosphere, as displayed in Fig. 3(b). Like the results obtained in air, the hydrogenated regions remain highly stable during heating. These results indicate that oxygen or moisture in the atmosphere would not have an impact on the stability of the protonated phase. Instead, the intercalated protons are energetically trapped within the YCO lattice through strong ion–lattice coupling, which effectively suppresses spontaneous dehydrogenation during thermal treatment. Furthermore, negligible lateral proton diffusion and excellent spatial confinement were also identified. It is noted that the sharp boundaries of written patterns were well preserved, which is critical for high-throughput device fabrication (Fig. 3(c)).[43] The temperature-dependent height and width evolution summarized in Fig. 3(d) further confirms the stability of the written HYCO phase. Moreover, when we placed the as-prepared HYCO sample in ambient air for 24 hours, it showed no detectable changes in the crystal structure and surface morphology (Fig. 3(e)). In Fig. 3(f), we compare the corresponding height profiles before and after storage, showing nearly overlapping curves with negligible height variation, which exhibits the nonvolatile retention behavior that is essential for synaptic weight storage in neuromorphic devices.[44]

3.4. Reversible writing and high-resolution nanoscale pattern fabrication

To further clarify the reversibility and cycling stability of proton modulation in YCO systems, tip-assisted localized hydrogenation and dehydrogenation processes were investigated. By controlling the polarity of the conductive AFM tip bias, reversible proton intercalation and extraction can be achieved, enabling programmable switching between different structural and electrical states at the nanoscale. As illustrated in Fig. 4(a), a 7×7 μm^2 region of the film surface was subjected to a $+7$ V for hydrogen intercalation, forming a uniformly elevated region. The corresponding height profile confirms a clear increase in surface thickness, indicating successful hydrogen incorporation. Subsequently, a 3×3 μm^2 central area within the protonated area was treated under -7 V to extract protons. As shown in Fig. 4(b), the central region recovered nearly to the original surface state, demonstrating that the proton-induced lattice expansion can be effectively reversed through electrically controlled dehydrogenation. This result directly proves that the hydrogenation process is not destructive but electrically reversible. Finally, a 1.5×1.5 μm^2 zone was further subjected to $+7$ V again for hydrogen intercalation, and local lattice expansion was restored (Fig. 4(c)). Furthermore, the recovered region still preserved clear boundaries, indicating that repeated hydrogen intercalation/extraction does not induce obvious structural degradation. The sequential hydrogenation–dehydrogenation–rehydrogenation process demonstrates highly reversible electrically programmable writing and erasing in YCO film. Such reversible structural modulation is particularly important for reconfigurable ion-related electronic devices and neuromorphic systems, where repeated state updating is essentially required.

Furthermore, the nanoscale patterning capability of the proton-writing process was also evaluated. Highly ordered mosaic nanostructures with extremely small feature sizes were fabricated, as shown in Fig. 4(d). The patterned regions exhibit clear periodic contrast and sharp boundaries without noticeable overlap between neighboring pixels, demonstrating excellent lateral confinement of proton diffusion. From the line profile extracted along the dashed line in Fig. 4(d), the periodic height modulation with distinct peaks and valleys can be clearly resolved, allowing quantitative evaluation of the lateral resolution (Fig. 4(e)). The minimum full width at half maximum reaches approximately 100 nm, which is comparable to the characteristic resolution achieved by conventional focused ion beam lithography or electron-beam patterning techniques, while avoiding severe physical damage associated with energetic particle bombardment.

Benefiting from the high spatial resolution, a complex programmable functional pattern was finally constructed. Figure 4(f) presents a quick response code fabricated through spatially selective proton injection. The distinct height contrast between hydrogenated and pristine regions enables reliable recognition of the encoded information using a smartphone or scanner, demonstrating the practical applications in information storage and encryption systems. These results collectively demonstrate that scanning-probe-induced hydrogen intercalation offers a highly controllable strategy for reversible nanoscale engineering of lattice structure and electronic states in correlated oxides. The demonstrated reversible atomic writing and high spatial resolution establish a solid physical foundation for reconfigurable circuits, artificial synapses, and intelligent sensing for oxide-based materials.

CPB Online First

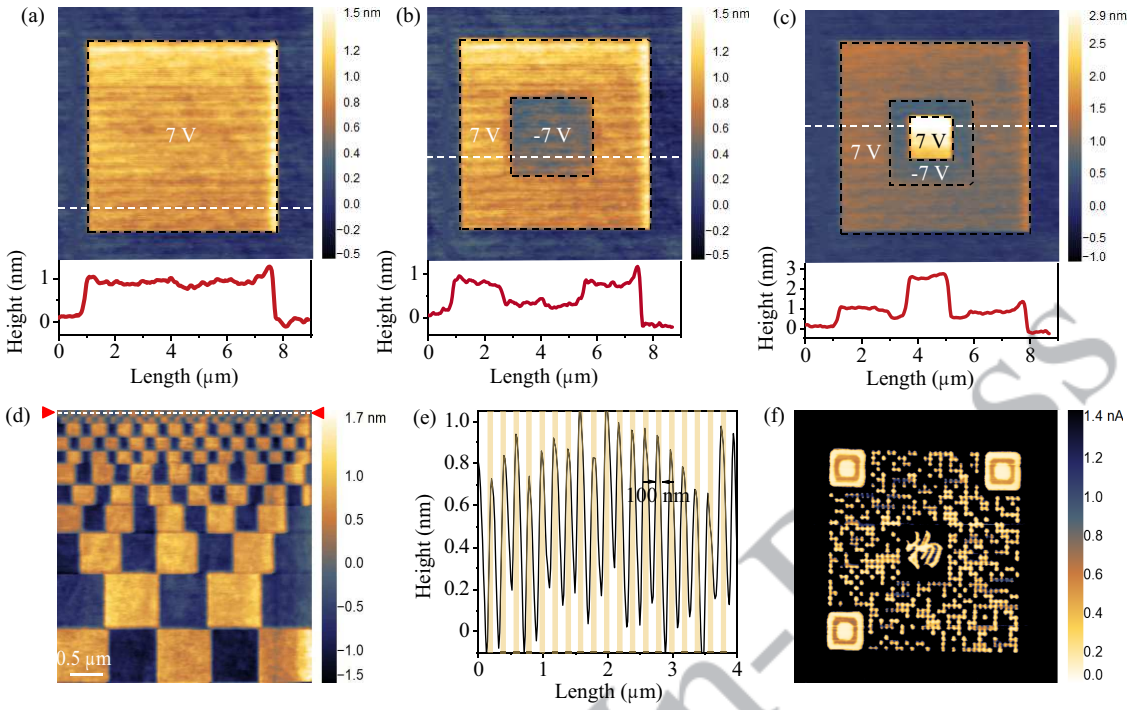


Fig. 4. Writing reversibility and identification of high spatial resolution. (a)–(c) Reversible hydrogen intercalation and extraction induced lattice expansion and reduction under scanning bias of +7 V and −7 V. (d) Height mapping of the designed high-resolution pattern. (e) Height profile along the white dashed line in (d), from which a 100 nm spatial resolution can be clearly identified. (f) Atomic probe written quick response code micropattern with distinct electrical conductance and surface morphology. The pattern size is 12×12 μm^2.

4. Conclusion

In summary, we systematically investigated the local electric-field modulation for nanopatterning and hydrogen ion control in YCO thin films. By precisely regulating the tip bias, reversible hydrogen intercalation and extraction were achieved with high spatial selectivity. This local ionic modulation induces a noticeable out-of-plane lattice expansion, accompanied by pronounced and controllable changes in electrical conductivity. High-resolution nanopatterns with well-defined boundaries can be directly written and erased without masks or complex lithographic processes. Moreover, the locally hydrogenated YCO regions exhibit excellent phase transition reversibility, spatial confinement, and thermal stability. In particular, the hydrogen-doped states remain highly stable, demonstrating nonvolatile retention behavior. This work provides a promising material platform for the fabrication of nano-electronic devices, neuromorphic synaptic arrays, and reconfigurable oxide electronic circuits.

Acknowledgements

This work was financially supported by the National Natural Science Foundation of China (Grant No. 52572146), the National Key R&D Program of China (Grant Nos. 2024YFA1408302 and 2022YFA1403000), the Beijing Nature Science Foundation (Grant No. Z250006), the CAS Project for Young Scientists in Basic Research (Grant No. YSBR-047), and the Key Scientific Research Project of the Education Department of Anhui Province (Grant No. 2025AHGXZK30856).

References

[1] Medarde M L 1997 *J. Phys.: Condens. Matter* **9** 1679
[2] Zhu Z L, Gua J H, Jia Y and Hu X 2010 *Phys. Status. Solidi. B* **247** 308
[3] Jia T, Hao Y N and Hao H 2024 *Results Phys.* **61** 107766
[4] Hashimoto H, Kusunose T and Sekino T 2009 *J. Alloys Compd.* **484** 246
[5] Girardot C, Kreisel J, Pignard S, Caillault N and Weiss F 2008 *Phys. Rev. B* **78** 104101
[6] Scherwitzl R, Zubko P, Lichtensteiger C and Triscone J M 2009 *Appl. Phys. Lett.* **95** 222114
[7] Alonso J A, Martínez L M J, Casais M T, Aranda M A G and Fernández D M T 1999 *J. Am. Chem. Soc.* **121** 4754
[8] Granados X, Fontcuberta J, Obradors X, Mañosa L and Torrance J B 1993 *Phys. Rev. B* **48** 11666
[9] Tomiyasu K, Sato M, Koyama S I, Nojima T, Kajimoto R, Ji S and Iwasa K 2017 *J. Phys. Soc. Jpn.* **86** 094706
[10] Murtaza G, Meraj M Usman, Hassan M, Younas M, Aloufi N M, Alhummiany H, Al-Anazy M M, Alshihri A A, Shah S T A and Mahmood Q 2024 *J. Mater. Sci: Mater. Electron.* **35** 1430
[11] Shin D, Yoon S, Song S, Park S, Lee H N and Choi W S 2022 *Adv. Mater. Interfaces* **9** 2200433
[12] Bisri S Z, Shimizu S, Nakano M and Iwasa Y 2017 *Adv. Mater.* **29** 1607054
[13] Terabe K, Tsuchiya T, Yang R and Aono M 2016 *Nanoscale* **8** 13873
[14] Nguyen T T N, Nguyen P K D, Luan V H, Do T M H, Tran V M, Tseng T H, Chang Y H, Nguyen M T K and Le M V 2026 *Colloid. Surf. A* **741** 140291
[15] Guo X, Tian Z X, Qu J C, Ye X, Wang L, Zhang Y M, Dong S T and Ju H B 2025 *J. Alloys Compd.* **1031** 181003
[16] Lu N P, Zhang P F, Zhang Q H, Qiao R M, He Q, Li H B, Wang Y J, Guo J W, Zhang D, Duan Z, Li Z L, Wang M, Yang S Z, Yan M Z, Arenholz E, Zhou S Y, Yang W L, Gu L, Nan C W, Wu J, Tokura Y and Yu P 2017 *Nature* **546** 124

CPB Online in Press

[17] Lu N P, Zhang Z, Wang Y J, Li H B, Qiao S, Zhao B, He Q, Lu S C, Li C, Wu Y S, Zhu M T, Lyu X Y, Chen X K, Li Z L, Wang M, Zhang J Z, Shen S C, Guo J W, Yang S Z, Zhang J B, Deng K, Zhang D, Ma J, Ren J, Wu Y, Zhu J Y, Zhou S Y, Tokura Y S, Nan C W, Wu J and Yu P 2022 *Nat. Energy* **7** 1208

[18] Prins R 2012 *Chem. Rev.* **112** 2714

[19] Zhu M T, Wang L, Gao L, Liu J, Lyu X Y, Wang Y Q, Lu C, Li M C, Liu P Y, Song J Y, Tao H Y, Zhao B B, Ji A L, Cao Z X and Lu N P 2025 *Chin. Phys. Lett.* **42** 037201

[20] Ha S D, Shi J, Meroz Y, Mahadevan L and Ramanathan S 2014 *Phys. Rev. Appl.* **2** 064003

[21] You Z and Ramanathan S 2015 *Proc. IEEE* **103** 1289

[22] Chen J K, Mao W, Gao L, Yan F B, Yajima T, Chen N F, Chen Z Z, Dong H L, Ge B H, Zhang P, Cao X Z, Wilde M, Jiang Y, Terai T and Shi J 2020 *Adv. Mater.* **32** 1905060

[23] Li J K, Ge C, Du J Y, Wang C, Yang G Z and Jin K J 2020 *Adv. Mater.* **32** 1905764

[24] Oh C, Jo M and Son J 2019 *ACS Appl. Mater. Interfaces* **11** 15733

[25] Zuo F, Panda P, Kotiuga M, Li J R, Kang M G, Mazzoli C, Zhou H, Barbour A, Wilkins S, Narayanan B, Cherukara M, Zhang Z, Sankaranarayanan S K R S, Comin R, Rabe K M, Roy K and Ramanathan S 2017 *Nat. Commun.* **8** 240

[26] Lyu X Y, Tao H Y, Yue J Y, Chu K, Niu Y J, Wang Q J, Wang L, Ji A L, Zhang Q H, Jiang P, Cao Z X, Lu N P 2026 *Chin. Phys. B* accepted

[27] Amarasinghe D K, Yu H M, Rodolakis F, Zhou H, Cao H and Ramanathan S 2022 *J. Solid. State. Chem.* **315** 123512

[28] Zhang F, Zhang Y, Li L L, Mou X, Peng H N, Shen S C, Wang M, Xiao K H, Ji S H, Yi D, Nan T X, Tang J S and Yu P 2023 *Nat. Commun.* **14** 3950

[29] Cen C, Thiel S, Hammerl G, Schneider C W, Andersen K E, Hellberg C S, Mannhart J and Levy J 2008 *Nat. Mater.* **7** 298

[30] Hanada A, Kinoshita K and Kishida S 2012 *Appl. Phys. Lett.* **101** 043507

[31] Li L L, Wang M, Zhou Y D, Zhang Y, Zhang F, Wu Y S, Wang Y J, Lyu Y J, Lu N P, Wang G P, Peng H N, Shen S C, Du Y G, Zhu Z H, Nan C W and Yu P 2022 *Nat. Mater.* **21** 1246

[32] Yang R 2020 *Chin. Phys. B* **29** 097305

[33] Zheng D F, Tian G, Wang Y D, Yang W D, Zhang L Y, Chen Z F, Fan Z, Chen D Y, Hou Z P, Gao X S, Li Q L and Liu J M 2022 *J. Materiomics* **8** 274

[34] Dey T, Lai X, Manna S, Patel K, Patel R K, Bisht R S, Zhou Y, Shah S, Andrei E Y, Sankaranarayanan S K R S, Kuzum D, Schuman C and Ramanathan S 2025 *ACS Nano* **19** 6815

[35] Zhang W H, Wu X Q, Wang W T, Zhang K D, Li B W and Chen Y H 2022 *ACS Appl. Electron. Mater.* **4** 2101

[36] Ohta H, Sato Y, Kato T, Kim S W, Nomura K, Ikuhara Y and Hosono H 2010 *Nat. Commun.* **1** 118

[37] Bi F, Bogorin D F, Cen C, Bark C W, Park J W, Eom C B and Levy J 2010 *Appl. Phys. Lett.* **97** 173110

[38] Evans D M, Holstad TS, Mosberg A B, Småbråten D R, Vullum P E, Dadlani A L, Shapovalov K, Yan Z, Bourret E, Gao D, Akola J, Torgersen J, Van H A T J, Selbach S M and Meier D 2020 *Nat. Mater.* **19** 1195

[39] Ferreiro V E, Blanco C S, Lucas D P I, Vasili H B, Magén C, Ibarra A, Rubio Z J, Castro G R, Morellón L and Rivadulla F 2019 *Adv. Funct. Mater.* **29** 1901984

[40] Katase T, Endo K, Tohei T, Ikuhara Y and Ohta H 2015 *Adv. Electron. Mater.* **1** 1500063

[41] Pellegrino L, Bellingeri E, Pallecchi I, Siri A S, Marr D and Chincarini A 2004 *J. Electroceram* **13** 331

[42] Zou J, Zeng H R, Wang Y C and Li Y X 2018 *Phys. Status. Solidi. RRL.* **12** 1700439

[43] Amdursky N, Lin Y Y, Aho N and Groenhof G 2019 *Proc. Natl. Acad. Sci. USA* **116** 2443

[44] Guo Y B and Zhu L Q 2020 *Chin. Phys. B* **29** 078502

CPB Online Last Press